Application of the extreme value theory to beam loss estimates in the SPIRAL2 linac based on large scale Monte Carlo computations

R. Duperrier and D. Uriot*

Laboratoire d'Étude et de Développement pour les Accélérateurs, CEA/DSM/DAPNIA/SACM, CEN Saclay 91191 Gif sur Yvette, France

(Received 23 November 2005; published 25 April 2006)

The influence of random perturbations of high intensity accelerator elements on the beam losses is considered. This paper presents the error sensitivity study which has been performed for the SPIRAL2 linac in order to define the tolerances for the construction. The proposed driver aims to accelerate a 5 mA deuteron beam up to 20 A MeV and a 1 mA ion beam for $q/A = 1/3$ up to 14.5 A MeV. It is a continuous wave regime linac, designed for a maximum efficiency in the transmission of intense beams and a tunable energy. It consists in an injector (two ECRs sources + LEBTs with the possibility to inject from several sources + radio frequency quadrupole) followed by a superconducting section based on an array of independently phased cavities where the transverse focalization is performed with warm quadrupoles. The correction scheme and the expected losses are described. The extreme value theory is used to estimate the expected beam losses. The described method couples large scale computations to obtain probability distribution functions. The bootstrap technique is used to provide confidence intervals associated to the beam loss predictions. With such a method, it is possible to measure the risk to loose a few watts in this high power linac (up to 200 kW).

I. INTRODUCTION

Once the reference design for the accelerator with perfect elements respects the requirements, it is necessary to evaluate the effects of imperfect elements. This evaluation permits one to define tolerances for the construction of the linac and to test the robustness of the achieved architecture. The design is assumed to be ''robust'' if the probability to record intolerable beam losses is a few percent. This robustness test may be compared to a risk measurement. By ''imperfect element,'' we mean for instance that we have to consider that the quadrupoles would not be at the correct position or that the cavities would not be at the right phase and so on and so forth. To correct such errors, a correction scheme based on correctors and diagnostics has to be designed taking into account that the diagnostics are also imperfect (misalignments, measurement, ...). Several authors studied the effects of imperfect ion linacs on the beam [1–6]. In Refs. [2,3], the effect of nonlinear space charge force is not treated. The halo induced by these effects is then underestimated and the loss prediction becomes distorted. The approach in [1] is helpful if the Coulomb force is negligible but is inaccurate for high power linac at low energy. To tend to ''realistic'' simulation of a high intensity linac, it is necessary to perform start-to-end transport to be capable of estimating the impact of halo produced at low energy on the beam losses at the high energy part of the accelerator. References [4–6] detail start-to-end simulations to take into account this point. In these references, the main mechanisms to produce the beam halo are the space charge and/or the nonlinear external fields. These studies used macroparticles to estimate beam distribution and to record the losses at the beam pipe. The discrete recorded losses at different locations in the linac allow one to build a cumulative distribution function (CDF) to provide a probability to deposit more than a certain fraction of beam. But the discrete form of this CDF induces that the probability to lose more than the more extreme recorded loss becomes null. We are not capable then to predict very extreme events. The extreme value theory provides a firm theoretical foundation to perform such a goal [Fisher and Tipett (1928) and Gnedenko (1943)]. Combining this theory with the bootstrap technique, we propose in this paper to detail a procedure to compute the average probability of occurrence of extreme events such as a very low beam loss (10^{-5}) including a confidence interval (error bar) associated to this evaluation. The procedure uses large scale simulations of linacs combining different sets of errors. The correction scheme manages the beam center and size. To illustrate the method, the SPIRAL2 linac is used. To estimate the relative impact of errors, the following section recalls the performances of the reference design of the driver.

*Electronic address: rduperrier@cea.fr, duriot@cea.fr

II. THE REFERENCE SIMULATION WITHOUT ERROR

A. Calculation framework

To compare with the results including the element errors, this paragraph shows a simulation of the reference design. This design has been presented at the EPAC 2004 conference [7]. A 1 300 000 macroparticle $4 \times \sigma$ Gaussian

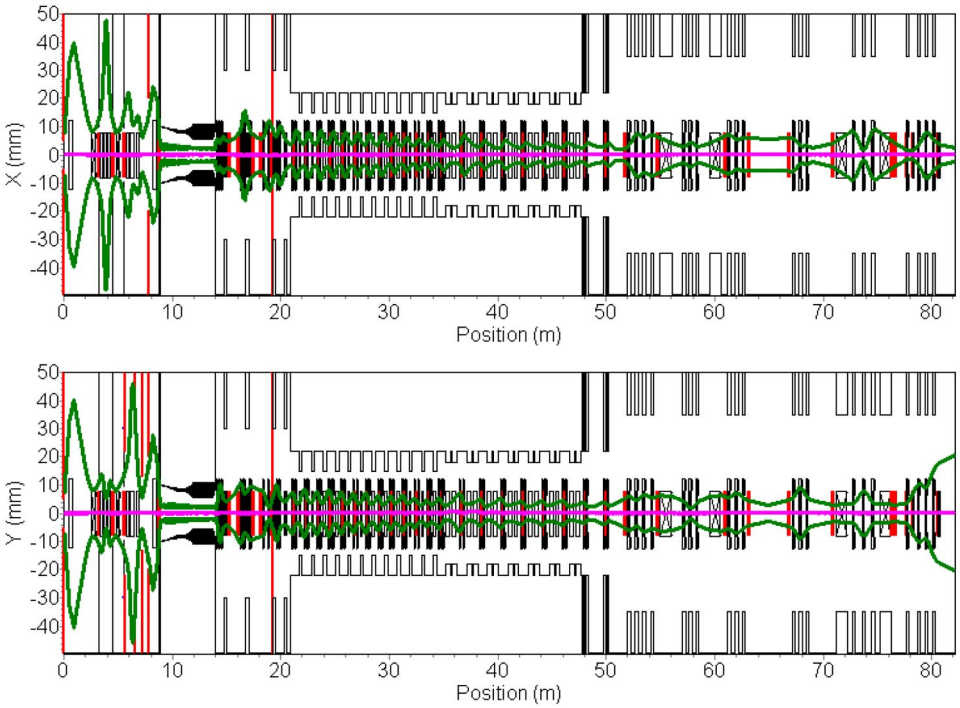

FIG. 1. (Color) The transverse envelope behavior for the deuteron beam in the SPIRAL2 linac ($\sqrt{5} \times \sigma$ which is equivalent to the size of an uniform distribution in position).

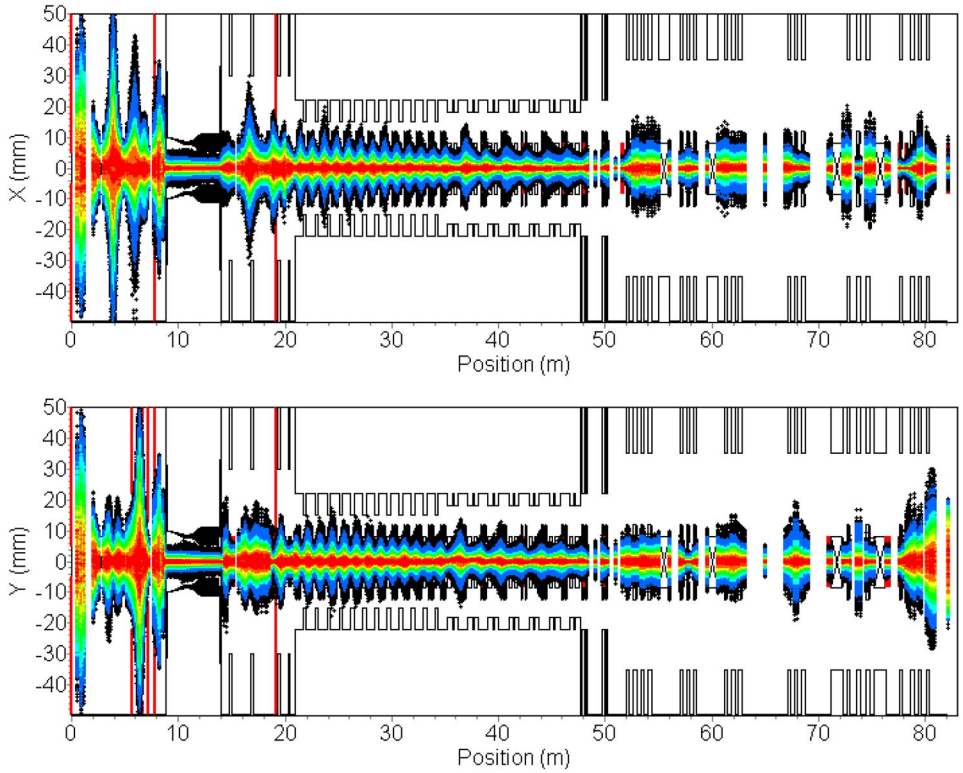

FIG. 2. (Color) The deuteron density projection in the transverse plane in the SPIRAL2 linac.

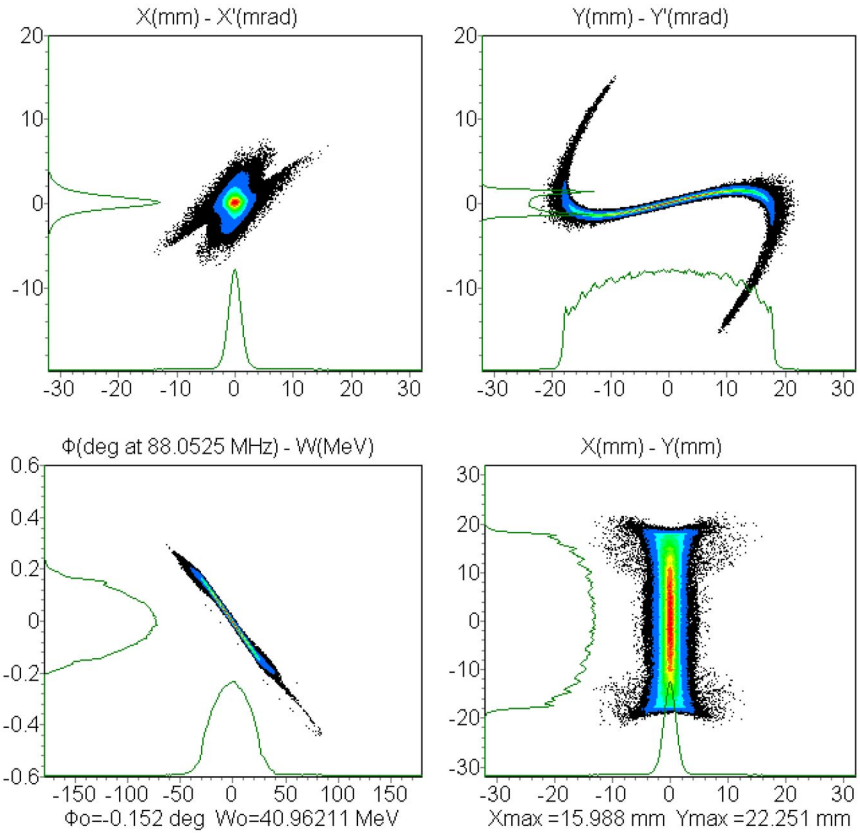

FIG. 3. (Color) The density portrait of the deuteron beam at the linac exit in the phase space.

distribution is used at the input of the LEBT line. The transverse rms normalized emittance used is 0.2π mm mrad. The beam current is 5 mA. A deuteron beam is considered to estimate the most critical beam losses. Multiparticle simulations are performed from the low-energy beam transport (LEBT) line to the target through the radio frequency quadrupole (RFQ), the medium energy beam transport (MEBT), the superconducting linac (SCL) and the high energy beam transport (HEBT) line. The transport of the beam through the RFQ is computed with the code TOUTATIS [8]. The rest of the linac is simulated with the TraceWin/PARTRAN package [9]. The space charge is calculated with the PICNIC routine[10] for Partran and a finite difference method for TOUTATIS [8]. The simulation takes into account a 3D domain and neighbor bunches. Several elements are simulated using a 3D field map: the LEBT quadrupoles, the RFQ and the quarter wave resonators. Preliminary studies have shown that the simulation of the other elements can be performed using the classical hard edge formalism. To manage the necessary huge number of runs for the Monte Carlo study, we implemented in Tracewin a software package that permits to pilot a heterogeneous collection of PCs [9]. The package is based on a client/server architecture to distribute the different independent runs. This is a multiparameter scheme and not a parallel scheme which is less optimal as each run can be performed by a single PC. As the communication between each node is minimum, the efficiency is enhanced. The envelope behaviors are plotted in Fig. 1. Figure 2 shows the beam density projection per plane in the linac. The density portrait in the phase space of the deuteron beam at the linac exit is shown in Fig. 3 and the rms evolutions are shown Fig. 4. The nonlinear space

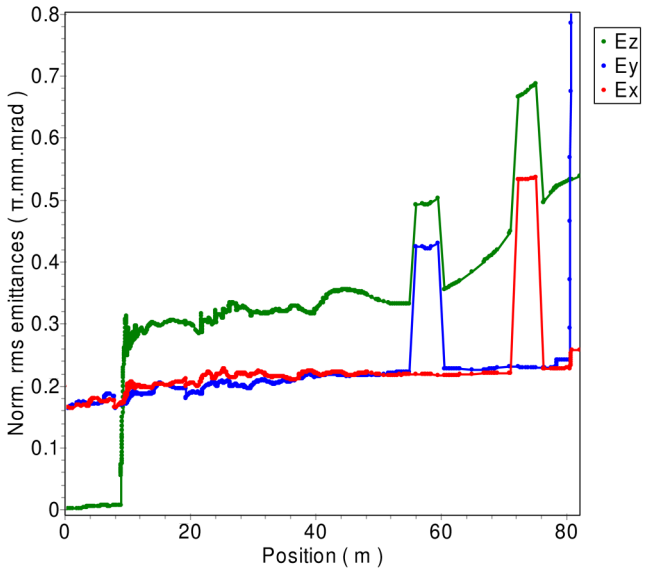

FIG. 4. (Color) Normalized rms emittance evolutions.

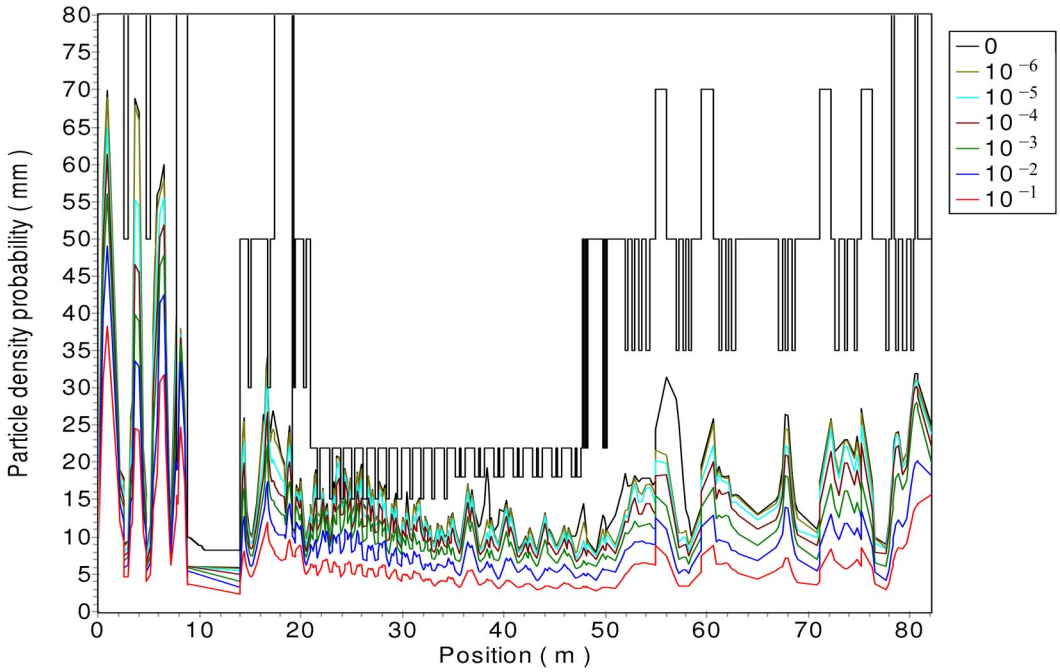

FIG. 5. (Color) Beam size radii along the linac. 10^{-1} corresponds to 90% of the beam, $10^{-2} \rightarrow 99\%$, $10^{-3} \rightarrow 99.9\% \ldots$ and the last black one is the radial aperture.

charge forces are the main source of the emittance growth. The phase dependent steering induced by the quarter wave resonators is negligible.

B. Beam losses

Figure 5 represents the different beam size radii along the linac (isodensity contours). The red line corresponds to 90% of the beam, the blue one 99%, the green 99.9%, ... and the last black line represents the aperture. We observe that the beam size is closer to the aperture in the first part of the superconducting accelerator. Figure 6 shows the losses which occur in the structure. Three main locations for the losses are observed. The first one (30 W) corresponds to a halo scraper located in the beginning of the LEBT. The second one (10 W) is due to the scraper which has to remove the chopped beam in the LEBT and to collimate the halo. The last one (160 W) is in the MEBT. This power is deposited on a scraper. This device has to protect the superconducting part from the beam halo coming from the MEBT. Without this collimator, more than 3 W are lost in the first superconducting cavities. The acceptable losses in the linac are defined in Table I. The SCL is divided in two parts, the warm one (quadrupoles, diagnostics, pumps) and the cold one (cryostats). They have been defined in respect to radioprotection and cryogenic efficiency considerations. The maximum beam power dissipated in each superconducting cavity has to be lower than 1 W to minimize the extra power.

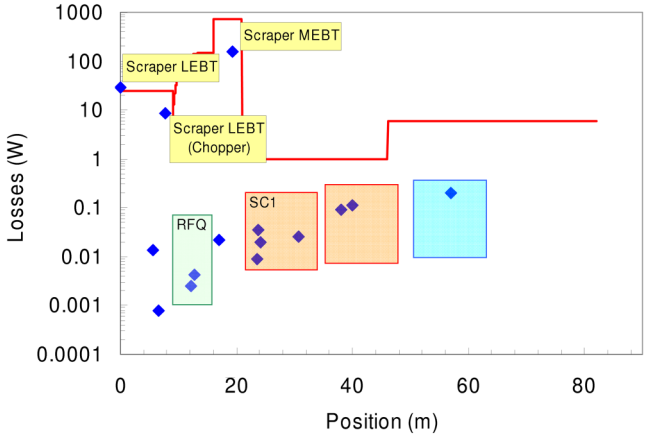

FIG. 6. (Color) Losses (W) along the structure, the loss limit requirements are the red line.

TABLE I. Loss tolerances. For the accelerating structures, the first value corresponds to the tolerance at the beginning of the structure and the last one to the end.

Section	Losses (%)	Losses (W)
LEBT	12.5	25
RFQ	2	$4 \rightarrow 150$
MEBT	10	730 W
SCL (warm)	$0.2 \rightarrow 0.003$	$4 \rightarrow 6$
SCL (cold)		1
HEBT	0.003	6

III. SENSITIVITY OF THE LINAC TO ELEMENT ERRORS

A. Definitions of errors and strategy

Before detailing different types of errors, it is important to remark that two families of errors have to be coped with

"Corrected" errors—These errors are applied before tuning the linac. They are, for instance, cavity and quadrupole misalignments or field errors. The tuning or "correction" of the linac is performed with steerers coupled with beam position monitors and quadrupoles coupled with profilers. The strategy of the correction scheme is established to minimize the effects of these static errors. The errors of the rf (field and phase) are also included in this category. They are not completely corrected because no longitudinal adjustment is applied, but the wrong transverse defocusing is readjusted with quadrupoles. Rotation around the beam axis of the quadrupoles is also included in this category but induced coupling is not corrected with a dedicated device, only the beam size readjustment is performed with the lenses.

Uncorrected errors.—These errors are applied after the correction procedure. They represent the dynamic fluctuations of the rf field or mechanical vibrations from the environment. Fortunately, these errors have usually lower amplitude but their frequencies may be problematic. In this study, we will not go into detail of this frequency problem. We will simulate the effect of uncorrected errors by adding them after correction of the static errors. These errors are mainly responsible for orbit oscillations around the corrected orbit. The notion of orbit is also extended to the longitudinal plane. The amplitudes of this defect are set to 1 order of magnitude lower than the static errors for transverse planes.

Depending on the linac section, errors with different amplitudes have been used. These amplitudes are summarized in Tables IX, X, XI, XII, XIII, and XIV in the appendix. For an error of amplitude A, the value has a uniform probability between $-A$ and $+A$. The rms value is then $A/\sqrt{3}$. If the distribution of errors is not uniform, the mechanical engineer will have to apply the principle of rms equivalence. The rotation angles around axes (OX, OY, OZ) are calculated with the following formulas:

$$\Theta_{x,y} = \frac{2d}{L} \quad \text{and} \quad \Theta_z = \frac{d}{R} \tag{1}$$

with d the displacement, L the length of the element, and R the aperture radius of the element. Usually, this kind of study combines different stages. First, each defect is studied separately and is amplified until an unacceptable threshold is reached. Second, the defaults are combined and amplified until the threshold is reached again. Weighting for the combination has to take into account relative sensitivity and the capacity to respect the induced tolerances. The main threshold for the SPIRAL2 project is to avoid losses in the superconducting section above 1 W per cavity. As this threshold is exceeded without error, the beam dump of the MEBT is also used as a scraper to control the loss level in the SC linac. Once the errors are included in the simulations, the losses can be still kept below 1 W per cavity. The new threshold would be the acceptable dissipated power on the MEBT collimator. As this threshold is unknown at this level of the project, study will lie in varying amplitudes of the errors described in Tables IX, X, XI, XII, XIII, and XIV all together from 0% to 200%. The dissipated power on the beam dump will be given for each amplitude of errors. These amplitudes of errors have been chosen after iterating with the engineering teams and the background from previous studies on high intensity linacs [11]. This background allowed us to avoid the preliminary studies to define the acceptable error for each element. The main strategy was to converge on values which may be reached with the present know-how in order to avoid an extra cost induced by R&D. This is the reason why, for example, the displacements in the cold part are around 1 mm compared to the warm part where they are around 0.1 mm.

B. Correction scheme

The beam center trajectory is controlled by using steerers which kick the beam in both planes. The transverse beam size is adjusted with quadrupoles coupled with beam profilers or an emittance measurement. Only data coming from diagnostics are used to tune the elements. With such a method, we are very close to the commissioning and tuning procedures which will be performed on the future machine. A description of the correction scheme for each section is given in Tables II, II, III, IV, and V and Fig. 7 illustrates the algorithm. The diagnostic errors are in Table VI.

C. Scan from 0% to 200% of errors

1. Results

The transport of 13 000 macroparticles has been simulated for each linac of a set of 100 different linacs in order

TABLE II. The correction scheme of the deuteron LEBT.

Correctors	Diagnostics
3 quadrupoles and 2 steerers	2 profilers (sizes and positions)
3 quadrupoles, 1 solenoid, and 2 steerers	Emittance measurement (sizes, divergences, positions, and angles); this measurement is used to match the beam at the RFQ entrance and control the beam position and angle.

TABLE III. The correction scheme of the MEBT.

Correctors	Diagnostics
3 quadrupoles and 2 steerers	2 profilers (sizes and positions)
3 quadrupoles and 2 steerers	2 profilers (sizes and positions)
1 steerer	1 beam position monitor (BPM)

TABLE IV. The correction scheme of the superconducting linac.

Correctors	Diagnostics
1 steerer for each of the 19 periods 4 last quadrupoles of the MEBT and the first one of the linac	Profilers for the 6 first periods and BPM at each period The matching procedure lies in adjusting these quadrupoles in order to get the same sizes in the horizontal and vertical planes. To avoid mismatching modes, this adjustment minimizes also the difference of sizes in a transverse plane from one period to the next one. This tuning is performed once the quadrupole channel is previously defined and only at the 6 first periods of the linac. It is not necessary to readjust any quadrupoles after this section because a continuity of the phase advance per meter has been set and makes that the linac is a single regular channel.

TABLE V. The correction scheme of the HEBT.

Correctors	Diagnostics
4 quadrupoles and 2 steerers	2 profilers (sizes and positions)
3 quadrupoles and 2 steerers	2 profilers (sizes and positions)
2 quadrupoles	2 profilers (sizes)
8 steerers	8 BPM

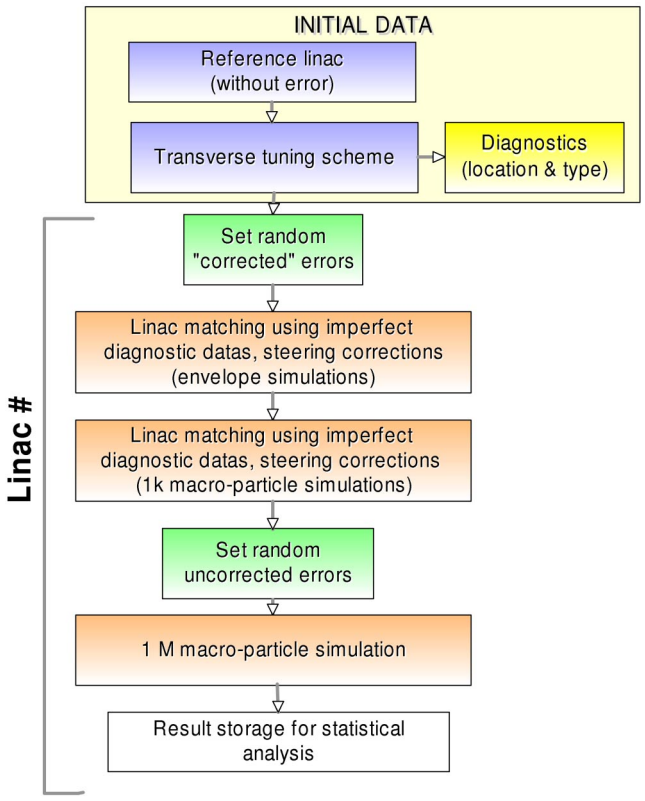

FIG. 7. (Color) The algorithm for each run which is launched on a node of the PC collection.

to get a convergence for the average losses. These average values will help us to select the acceptable tolerances for the SPIRAL2 driver. For each linac, all the errors are combined. Only the deuteron beam is simulated as it is assumed to be the more problematic one with respect to radioprotection. All plots show the mean values of each set of 100 linacs. To compute the linear density of the deposited power, total power in a section is divided by the total length of the section.

A power of 40 W is dissipated in the scrapers of the LEBT. This power is hardly sensitive to the errors. Figure 8 shows the losses for different amplitudes of errors. The collimators are excluded. It appears that the losses in the vacuum chamber of the LEBT do not significantly increase with the errors. The main reason is that the cumulative effect of imperfections is weak (beginning of the linac).

Comparing to Fig. 9 and Table I, the RFQ of the SPIRAL2 project appears to have a large acceptance. Losses are always kept below 1 W/m.

The two charts in Fig. 10 show the losses in the MEBT line. They are always lower than the radioprotection threshold (see Table I). But, the deposited power on the scraper located at the end of the line increases quickly. One option would be to multiply the number of scrapers to minimize the power per unit. It would perform also a more efficient scraping of the halo as one collimator will

TABLE VI. The amplitudes of errors for the diagnostics.

Element	Error	Value
BPM	Position accuracy (mm)	± 0.1
Profiler	Size accuracy (mm)	± 0.1
Emittance measurement	Size accuracy (%)	± 10
	Divergence accuracy (%)	± 10
	Position accuracy (mm)	± 0.1
	Angle accuracy (mrad)	± 0.3

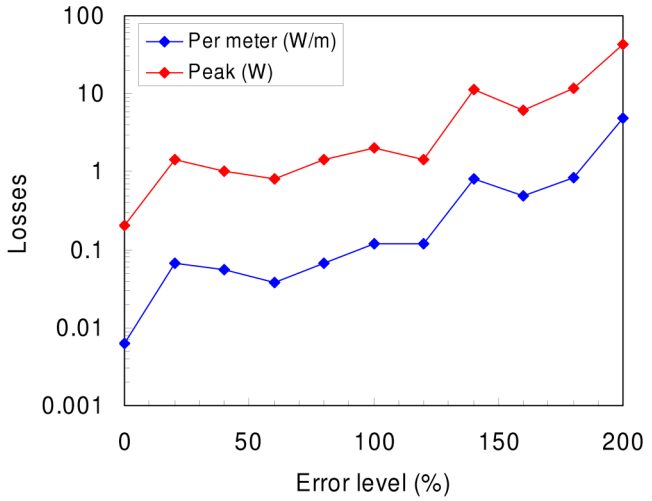

FIG. 8. (Color) The losses in the deuteron LEBT in respect to the error level.

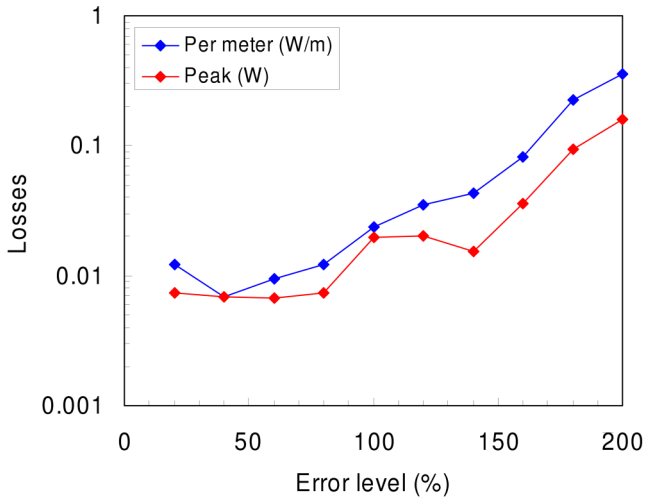

FIG. 9. (Color) The deuteron losses in the RFQ in respect to the error level.

not remove the halo particles which are crossing the axis at the scraper location. Calculations have been performed to verify that the loss level in SCL is tunable with the collimator aperture as much as the errors in the SCL itself are sufficiently weak.

The losses in the cavities for the first family of the SCL are always lower than 1 W (see Fig. 11). The main dissipated power is located in the first quadrupole (see Fig. 12). In the second SC family, the 1 W threshold is reached at ~150%.

Acceptable mean peak losses lower than 6 W are recorded if the amplitude of combined errors are lower than 140%. The behavior of losses in this line in respect to the error level is plotted in Fig. 13.

Figure 14 shows the losses and emittance growths for the whole linac without error as reference (see Sec. II).

2. Conclusion for the scan from 0% to 200% of error amplitude

All these results show that SPIRAL2 requirements are respected if the amplitudes of errors are lower than 140% if we consider mean values. A safer approach would be to choose an amplitude equal to 100% as a good compromise to minimize constraint for a possible upgrade to 100 MeV/u. The following section shows detailed results for this case.

D. Application of the extreme value theory for the loss estimate

1. Introduction

To get a good estimate of the distributions of centers in phase space plane, 10 000 macroparticles per run are largely sufficient. The most important quantity to reach convergence for the standard deviation is the total number of generated linacs. 1000 different linacs with all combined errors on each element have been used for this study.

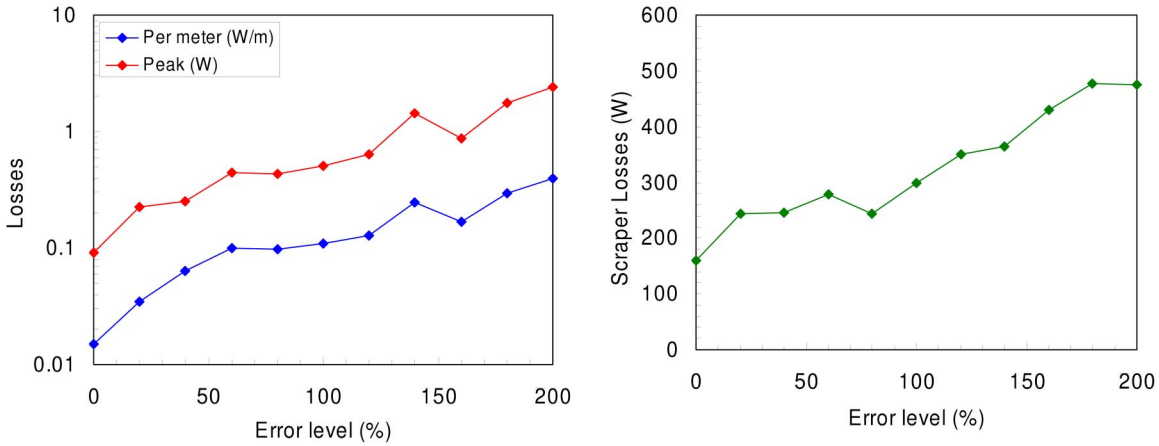

FIG. 10. (Color) The deuteron losses in the MEBT without the scraper and the deposited power on the scraper in respect to the error level.

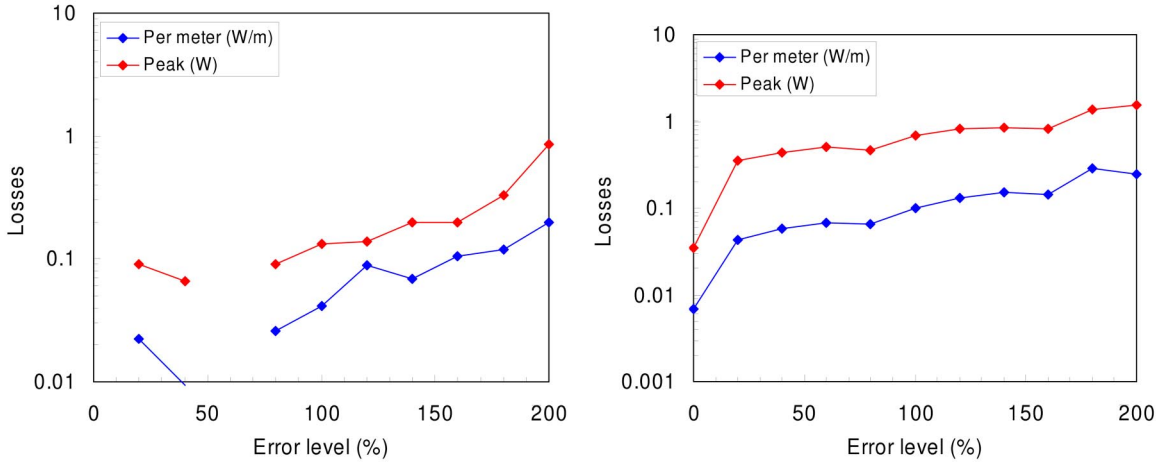

FIG. 11. (Color) The deuteron losses in the SC cavities in respect to the error level (first and second family of β).

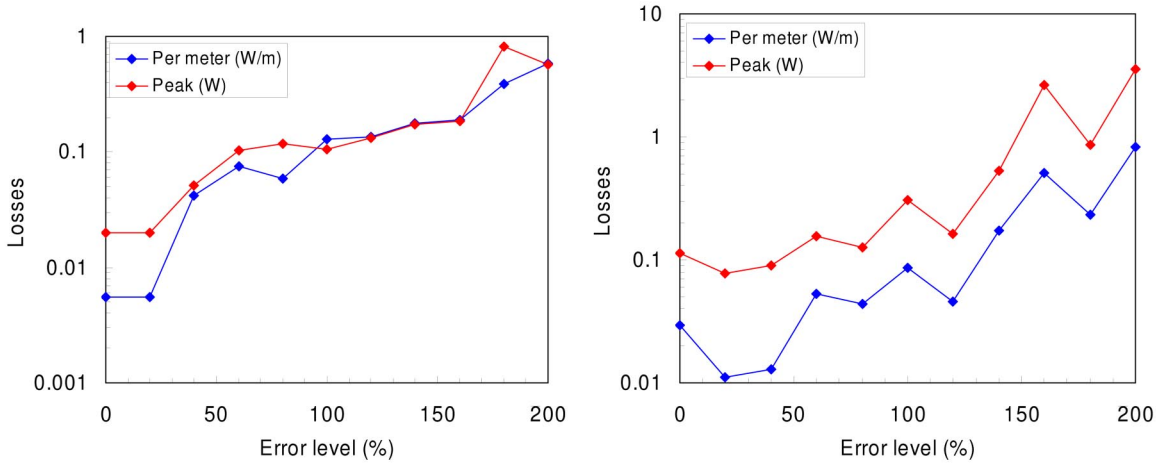

FIG. 12. (Color) The deuteron losses in the SCL warm part in respect to the error level (first and second family of β).

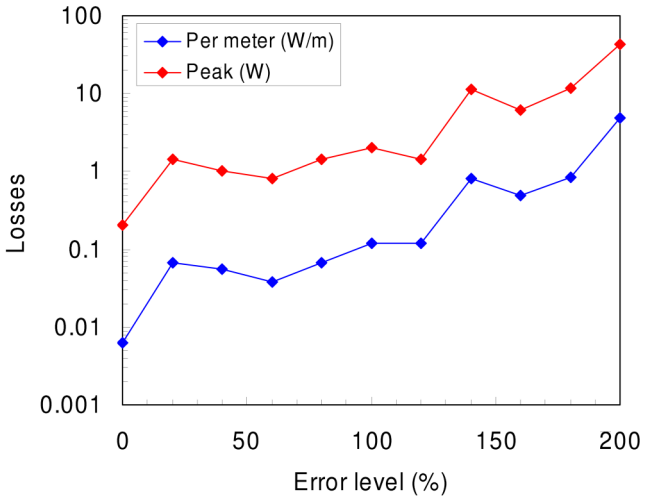

FIG. 13. (Color) The deuteron losses in the HEBT line in respect to the error level.

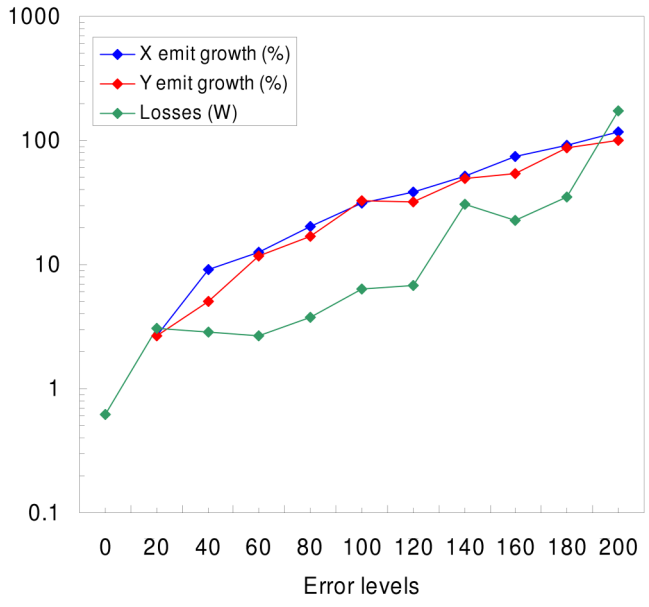

FIG. 14. (Color) The deuteron losses and rms emittance growths in the whole linac in respect to the error level (the whole linac without error is the reference).

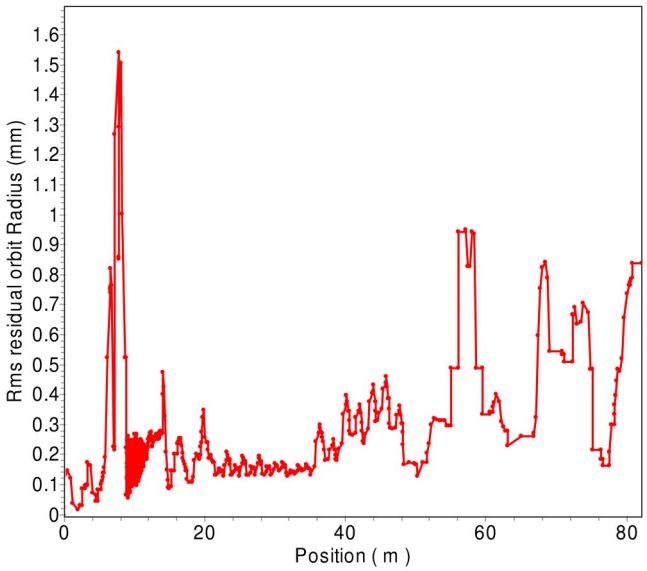

FIG. 15. (Color) rms orbit behavior in the linac.

The rms value of the orbit along the linac is plotted on Fig. 15. We notice that the rms jitter centroid position at the target is about 0.9 mm for this linac. It is mainly due to the dynamic errors (vibrations) and BPM accuracy. Figures 16 and 17 show the distributions of the centers for the 1000 linacs.

The distribution in Fig. 18 is the normalized superposition of 1000 different beams at the linac exit. It represents a probability contour map to reach this density at the target.

To study more precisely the losses occurring in the linac, the 10 000 macroparticles are not enough to estimate losses lower than 1 W for each linac. Thus, the number of particles per run has been increased to 1×10^6 in order to reach the required resolution and the number of run has been decreased to 341 runs (2 weeks of computations with 10 PCs). Figure 19 shows the statistical distribution of the particles all along the linac for 100% of errors. It is interesting to compare it with Fig. 5 to visualize the impact of errors on the halo.

This set of simulations provides data which can be used to build statistical models describing the extreme events. Extreme value theory (EVT) provides a firm theoretical foundation to perform such a goal. In many field of modern science, EVT is well established [12–14]. This paper will not detailed this theory. See the reference [14] which reviews the basics and illustrates EVT with examples. By "extreme events," in our case, we mean that we want to be able to provide the probability to loose more than 1 or 10 W, and so on and so forth with a confidence interval. To model the tails of our deposited beam power in the SPIRAL2 linac, we will apply the following method:

(i) First, scan the mean deposited power for each element of the accelerator to detect the most critical components
(ii) Second, fit the data with the Generalized Extreme Value (GEV) distribution.
(iii) Third, estimate confidence intervals for value of interest with the bootstrap method.

2. Average loss scan to select the hot spots

Figure 20 shows the mean losses repartition along the structure for the 341 linacs and the corresponding dissipated power. The repartition along the linac parts is summarized in Table VII. The *losses* column summarizes the integrated and the mean dissipated power along each machine section. The *peak power* column represents the average maximum dissipated power which occurs in one element of the section. For the SC linac, the warm part and the cold part have been separated. These last data allow us to select the most critical component in a particular section. This selection assumes that the higher average deposited power the higher the rms beam loss power for a given

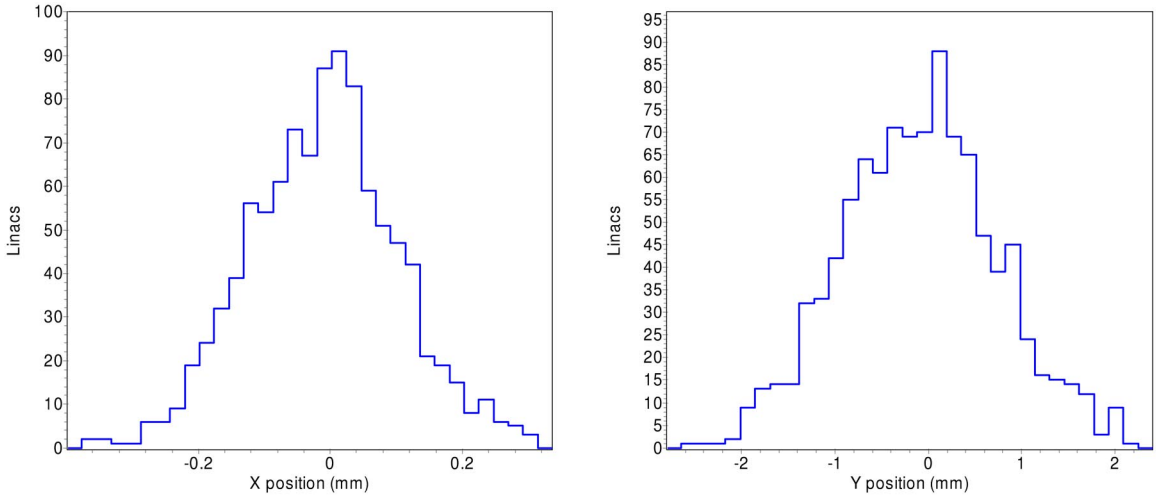

FIG. 16. (Color) Distributions for the position centers at linac exit (1000 simulations).

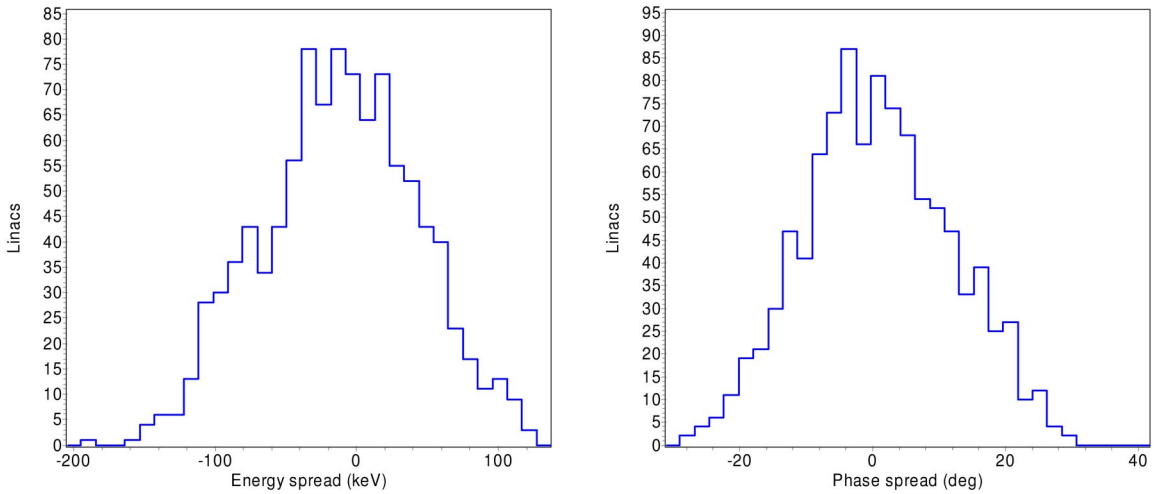

FIG. 17. (Color) Energy and phase distributions at linac exit (1000 simulations).

probability. The application of the extreme value theory is justified to study our problem (see below). The power distribution probability function is well represented by the Fréchet function of the variable (power $-\ \mu)/\sigma$, where μ is a location parameter and σ is a scale parameter. The mean value for such function is the sum $(\mu + \sigma\gamma)$ where γ is the Euler-Mascheroni constant (~ 0.6). The standard deviation is equal to $\sim 1.26 \times \sigma$. It means that we can reasonably expect that elements with a high standard deviation have also a high mean value.

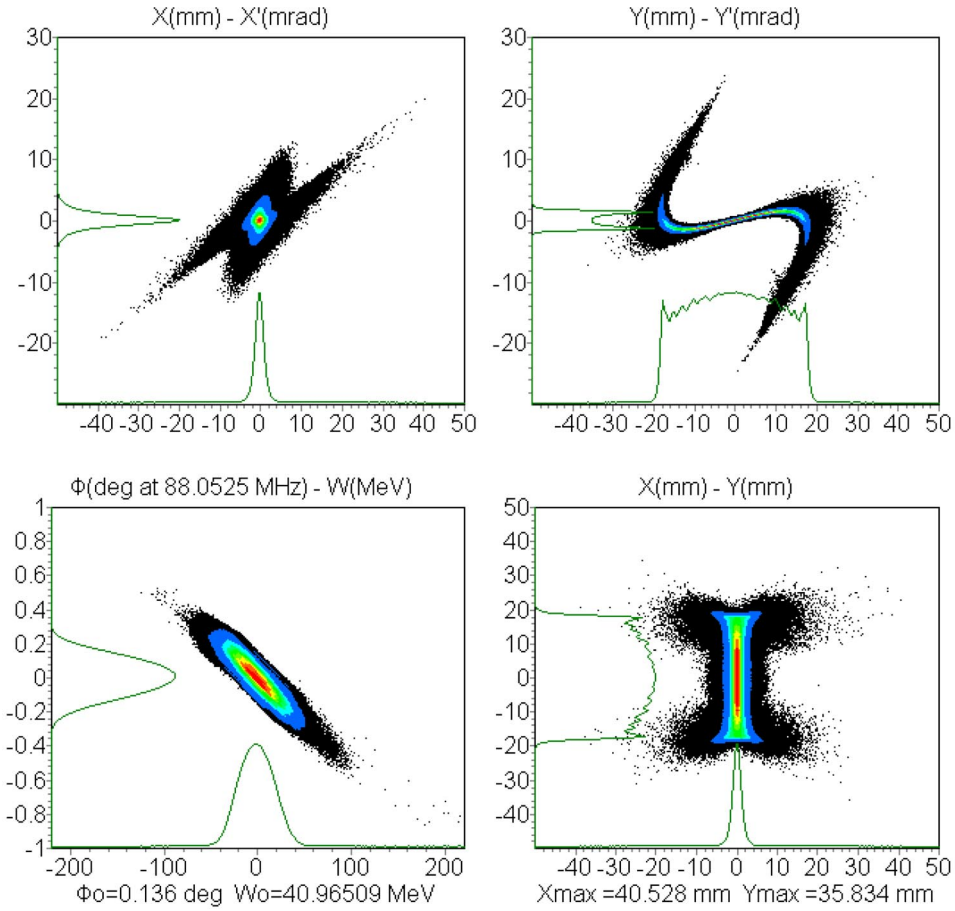

FIG. 18. (Color) The probability distribution contour map obtained by the normalized superposition of the 1000 output beam distributions.

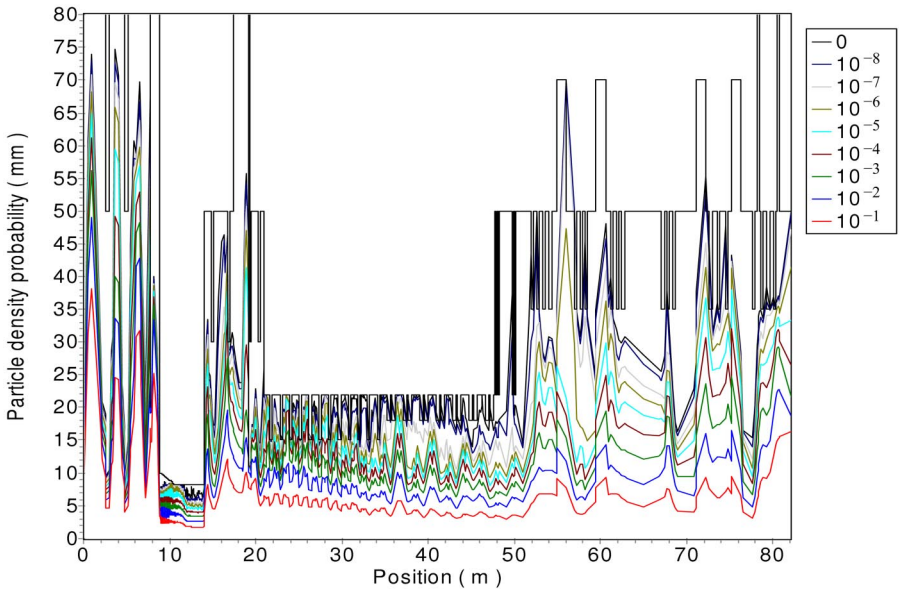

FIG. 19. (Color) Beam size radii along the linac. 10^{-1} corresponds to 90%and the last black one is the aperture.

If we focus on the results for the SCL, we can observe two critical elements. The first one is the first quadrupole of the first superconducting section where a mean value of 0.61 watt is dissipated and the second one is the first cavity of the $\beta = 0.12$ section where a mean power of 0.19 W is recorded. We will concentrate our study on these two elements.

3. *First quadrupole of the* $\beta = 0.07$ *section*

Figure 21 shows the recorded loss distribution at the first quadrupole of the first superconducting section. This represents the unnormalized probability density function (PDF) computed with the results of the 341 linacs with 1×10^6 simulated macroparticles per linac. With this number of macroparticles, one particle represents ~8 mW at this location of the linac.

Using this unormalized PDF, we can build a cumulative distribution function (CDF) which will be our reference data to fit with the GEV function of the lost power p:

$$H_{\xi\sigma\mu}(p) = \exp\left[-\left(1 + \xi\frac{p-\mu}{\sigma}\right)^{-1/\xi}\right], \qquad (2)$$

with μ, the location parameter, σ, the scale parameter and ξ, the Jenkinson and von Mises parameter. To build the CDF, we used the following formula:

$$F_n(x_i^n) = \frac{i}{n} \quad \text{for } i = 1, \ldots, n, \qquad (3)$$

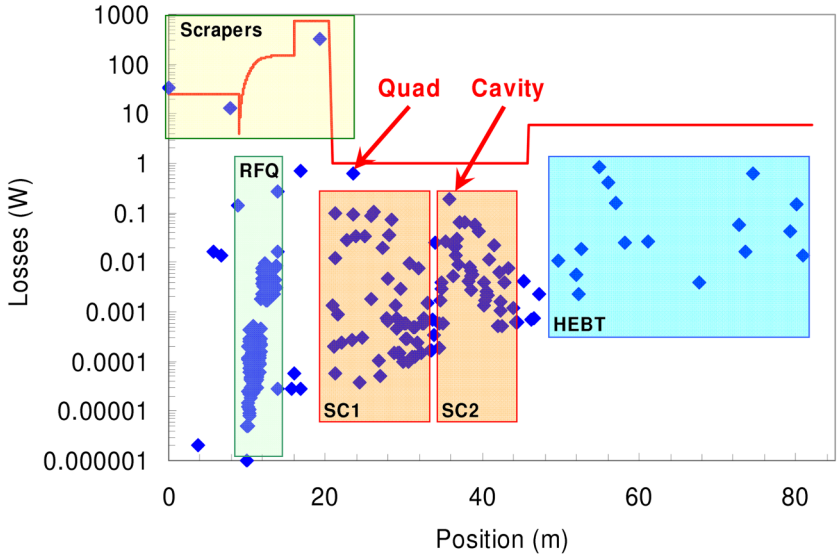

FIG. 20. (Color) Average loss repartition along the structure. The most critical components are pointed with red arrows.

TABLE VII. Average losses repartition according to linac section (ndy means "not designed yet").

	Losses (W)	Length (m)	Losses (W/m)	Peak losses (W)
LEBT	0.17	8.86	0.02	0.14
Scrapers LEBT	46.91	ndy		33.85
RFQ	0.33	5.09	0.07	0.14
MEBT	0.96	7	0.14	0.69
Scraper MEBT	317.23	ndy		317.23
SCL1 (warm)	0.97	10.2	0.09	0.61
SCL2 (warm)	0.160	7.014	0.02	0.03
SCL1 (cold)	0.34	3.6	0.09	0.10
SCL2 (cold)	0.50	6.986	0.07	0.19
HEBT	2.41	33.1	0.073	0.85

which is the sample distribution function for a set of n observations, given in increasing order $x_1^n \leq \cdots \leq x_i^n$. For our case, n is equal to 341. The GEV fitted with these data is plotted in Fig. 22. At this location of the linac, the requirements assume that less than 4 W should be deposited on the pipe. With the fitted GEV, we can estimate that the probability to loose less than 4 W is 0.97 which is very comfortable. The fitted parameters are $\hat{\xi} = 0.223$, $\hat{\sigma} = 0.89$, and $\hat{\mu} = -0.86$. To see how sensible is this result in respect to the achieved statistics, we can calculate a confidence interval at 95%. The bootstrap method is a helpful technique to construct such confidence interval. We resampled 1000 times the recorded PDF and recomputes the expected return power level for a probability of 0.97. Figure 23 shows the empirical bootstrap distribution for the return level for this probability. The confidence interval at 95% is then $[2.3; 5.9]$ W. This indicates that the recorded losses are sufficiently numerous to estimate that, with a good accuracy, we kept the beam losses at an acceptable level. If we need to estimate probability for very high loss level, the same procedure has to be repeated. For instance, with the same set of events, we can estimate that for a probability of occurrence of 10^{-4} the mean deposited power is 36 W with a confidence interval at 95% which is $[20; 52]$ W. It indicates that more recorded losses are required if we need to shrink the confidence interval around this mean value of 36 W.

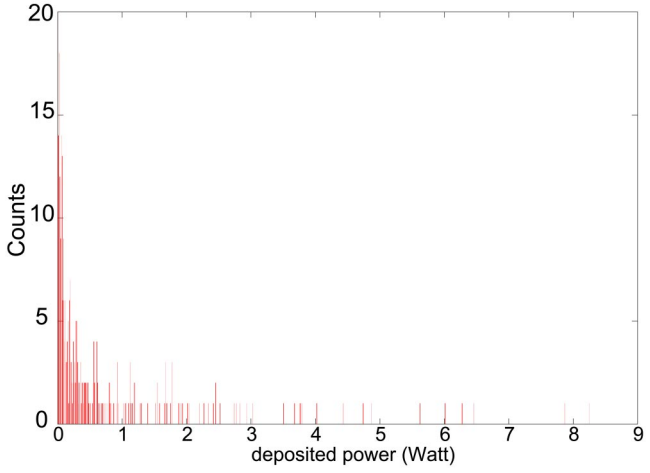

FIG. 21. (Color) Unnormalized probability density function for the losses at the first quadrupole of the first section. The deposited beam power (W) forms the abscissa and the number of counts the ordinate.

4. First cavity of the $\beta = 0.12$ section

With the same procedure, we can construct a GEV function fitted with the recorded losses at the cavity location. Figure 24 shows the fitted GEV with the recorded losses at the cavity location. The fitted parameters are $\hat{\xi} = 0.465$, $\hat{\sigma} = 0.062$, and $\hat{\mu} = -0.061$. The probability to loose less than 1 W is 0.99. With the bootstrap method, we can estimate a confidence interval for this probability. It is $[0.44; 1.33]$ W. Figure 25 illustrates the empirical bootstrap distribution for the return level for this probability. Table VIII gives a summary of the results for the most lossy quadrupole and cavity. To give an other example of the main interest to use EVT, we are capable to estimate that the probability to loose more than 10 W in this cavity is $8 \cdot 10^{-5}$.

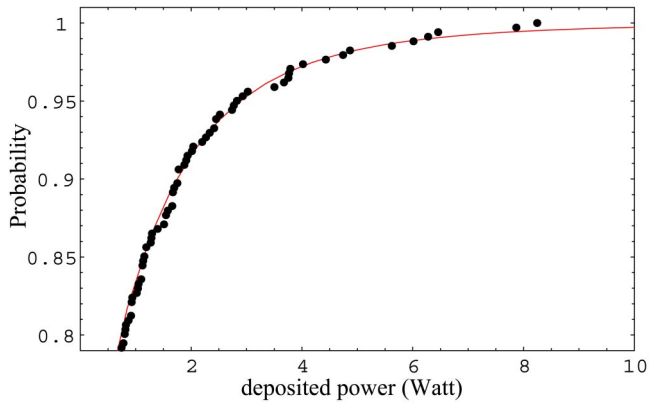

FIG. 22. (Color) GEV fitted with the recorded losses for the quadrupole. The deposited beam power (W) forms the abscissa and the CDF the ordinate.

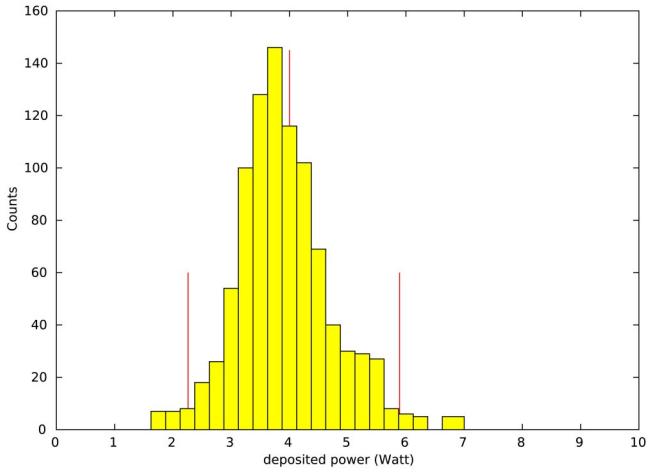

FIG. 23. (Color) Empirical bootstrap distribution for the return level with a probability of 0.97. The two small red marks indicate the $\pm 2\sigma$ interval, the big red mark indicates the return level obtained with a direct estimate from the recorded losses.

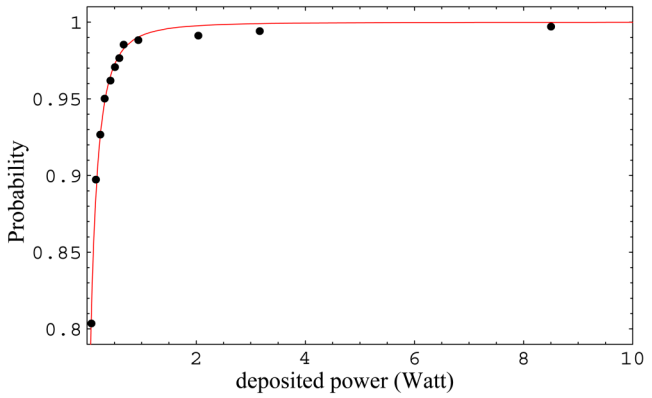

FIG. 24. (Color) GEV fitted with the recorded losses for the most critical cavity. The deposited beam power (W) forms the abscissa and the CDF the ordinate.

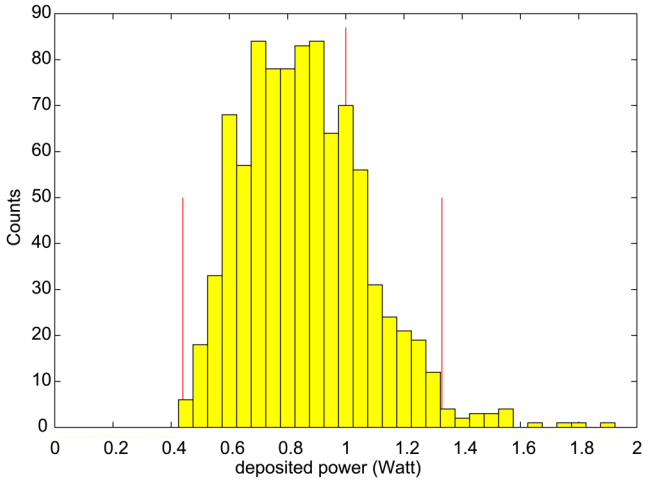

FIG. 25. (Color) Empirical bootstrap distribution for the return level with a probability of 0.99. The two small red marks indicate the $\pm 2\sigma$ interval, the big red mark indicates the return level obtained with a direct estimate from the recorded losses.

TABLE VIII. Beam loss estimates (PE) and 95% bootstrap confidence intervals.

	CDF @ PE	Lower bound	Point estimate (PE)	Upper bound
Quadrupole (W)	0.97	2.3	4	5.9
Cavity (W)	0.99	0.44	1	1.33

IV. CONCLUSIONS

This application of the extreme value theory to beam loss estimates in the SPIRAL2 linac based on large scale Monte Carlo computations allowed us to provide loss probability for this linac. The start-to-end error study show manageable losses with a $4 \times \sigma$ Gaussian as input distribution and the use of collimators. The probability to loose more than 1 W in a superconducting cavity predicted with the GEV is less than 10^{-2}. Such an event will happen on average one linac over 100 built linacs. The losses in the superconducting section are directly linked with the MEBT scraper while the amplitude of the errors in the SCL itself are not too large. Considering about 200 W of power dissipated on the MEBT scraper, the element tolerances are compatible with the present state of art. To go further to realistic estimates of the beam loss, a more faithful modelization of the linac is required. For instance, the output beam distribution of the ECR source is necessary to enhance the start-to-end modelizations and the beam interaction with the residual gas (neutralization) has to be taken into account to simulate more accurately the space charge force especially at low energy.

APPENDIX: AMPLITUDE ERROR TABLES

Depending on the linac section, errors with different amplitudes have been used. These amplitudes are summa-

TABLE IX. The amplitudes of errors for the RFQ cavity.

Error	Corrected	Uncorr.
Machining transv. curvature defect (mm)	± 0.1	0
Machining long. curvature defect (mm)	± 0.1	0
$\perp$ tilt by segment (mm)	± 0.1	± 0.01
$\parallel$ tilt by segment (mm)	± 0.1	± 0.01
$\perp$ displacement by segment (mm)	± 0.1	± 0.01
$\parallel$ displacement by segment (mm)	± 0.1	± 0.01

TABLE X. The amplitudes of errors for the magnetic quadrupoles.

Error	Corrected	Uncorrected
Gradient (%)	± 1	± 0.1
Displacement (mm)	± 0.1	± 0.01
Rotations (OX, OY) (deg.)	$\pm\Theta_{x,y}$	$\pm 0.1 \times \Theta_{x,y}$
Rotations (OZ) (deg.)	$\pm\Theta_{z}$	$\pm 0.1 \times \Theta_{z}$

rized in Tables IX, X, XI, XII, XIII, and XIV that follow.

TABLE XI. The amplitudes of errors for the magnetic dipoles.

Error	Corrected	Uncorrected
Field (%)	± 1	± 0.1
Displacement (mm)	± 0.1	± 0.01
Rotations (OX, OY) (deg.)	$\pm\Theta_{x,y}$	$\pm 0.1 \times \Theta_{x,y}$
Rotations OZ (deg.)	$\pm\Theta_{z}$	$\pm 0.1 \times \Theta_{z}$

TABLE XII. The amplitudes of errors for the buncher cavities.

Error	Corrected	Uncorrected
Amplitude (%)	± 1	± 0.1
Phase (deg.)	± 1	± 0.1
Displacement (mm)	± 1	± 0.1
Rotations (OX, OY) (deg.)	$\pm\Theta_{x,y}$	$\pm 0.1 \times \Theta_{x,y}$

TABLE XIII. The amplitudes of errors for the SC cavities.

Error	Corrected	Uncorrected
Amplitude (%)	± 1	± 0.1
Phase (deg.)	± 1	± 0.1
Displacement (mm)	± 1	± 0.1
Rotations (OX, OY) (deg.)	$\pm\Theta_{x,y}$	$\pm 0.1 \times \Theta_{x,y}$

TABLE XIV. The amplitudes of errors for the magnetic octupoles.

Error	Corrected	Uncorrected
Field (%)	± 1	± 0.1
Displacement (mm)	± 0.1	± 0.01
Rotations (OX, OY) (deg.)	± 0.04	± 0.004
Rotations (OZ) (deg.)	± 0.15	± 0.015

[1] B. P. Murin, B. I. Bondarev, A. P. Durkin, and L. YU. Soloviev, Part. Accel. **6**, 27 (1974).

[2] K. R. Crandall, in *Proceedings of the 1988 Linear Accelerator Conference, Williamsburg, VA* (Continuous Electron Beam Accelerator Facility, Newport News, VA, 1989), p. 335.

[3] D. Raparia *et al.*, in *Proceedings of the Particle Accelerator Conference, Washington, DC, 1993* (IEEE, Piscataway, NJ, 1993), p. 3585.

[4] N. Pichoff, R. Duperrier, and D. Uriot, in *Proceedings of the Particle Accelerator Conference, Chicago, IL. 2001* (IEEE, Piscataway, NJ, 2001), pp. 2869–2871.

[5] N. Pichoff, R. Duperrier, D. Uriot, and R. Ferdinand, in *Proceedings of the 8th European Particle Accelerator Conference, Paris, 2002*, pp. 1335–1337.

[6] P. N. Ostroumov, V. N. Aseev, and B. Mustapha, Phys. Rev. ST Accel. Beams **7**, 090101 (2004).

[7] R. Duperrier, in *Proceedings of the European Particle Accelerator Conference, Lucerne, 2004* (EPS-AG, Lucerne, 2004).

[8] R. Duperrier, Phys. Rev. ST Accel. Beams **3**, 124201 (2000).

[9] R. Duperrier, N. Pichoff, and D. Uriot, in *Proceedings of the International Conference Computational Science: ICCS 2002, Amsterdam, the Netherlands, 2002* (Springer-Verlag, Berlin, 2002).

[10] N. Pichoff *et al.*, in *Proceedings of the International LINAC Conference, Chicago, IL, 1998* (Argonne National Lab., Chicago, 1998), p. 141.

[11] R. Duperrier, J. Payet, and D. Uriot, in *Proceedings of the European Particle Accelerator Conference, Lucerne, 2004* (EPS-AG, Lucerne, 2004).

[12] P. Embrechts, C. Kluppelberg, and T. Mikosch, *Modelling Extremal Events for Insurance and Finance* (Springer-Verlag, Berlin, 1999), 2nd ed.

[13] Henri Klajnmic, in *XXXVIèmes Journées de Statistiques, Montpellier, France, 2004*, http://www.agro-montpellier.fr/sfds/CD/textes/klajnmic1.pdf

[14] M. Gilli and E. Kélezi, "An Application of Extreme Value Theory for Measuring Risk," http://www.unige.ch/ses/metri/gilli/evtrm/GilliKelleziEVT.pdf